Applied Catalysis B: Environmental 199 (2016) 55–63

Contents lists available at ScienceDirect

Applied Catalysis B: Environmental

journal homepage: www.elsevier.com/locate/apcatb

Size-dependent plasmonic effects of Au and Au@SiO_2 nanoparticles in photocatalytic CO_2 conversion reaction of Pt/TiO_2

Sandipan Bera, Ji Eun Lee, Sher Bahadur Rawal, Wan In Lee*

Department of Chemistry and Chemical Engineering, Inha University, Incheon 402-751, Republic of Korea

ARTICLE INFO

Article history:
Received 25 April 2016
Received in revised form 4 June 2016
Accepted 7 June 2016
Available online 8 June 2016

Keywords:
Plasmonic photocatalyst
CO_2 conversion
Pt/TiO_2
Au nanoparticle
Au@SiO_2 nanoparticle

ABSTRACT

Au nanoparticles (NPs) with sizes of 4, 8, 18 and 26 nm, as well as their corresponding Au@SiO_2 core-shell NPs, were selectively synthesized. The prepared plasmonic NPs were loaded onto Pt/TiO_2 in order to investigate their size-dependent plasmonic effect in the photocatalytic CO_2 conversion reaction. In evolving CH_4 from CO_2 under 365 nm LED lamp irradiation, the loading of the Au or Au@SiO_2 NPs does not appreciably influence the photocatalytic activities of Pt/TiO_2, whereas under the co-irradiation of 365 and 530 nm LED lamps, their photocatalytic activities are remarkably increased, clearly indicating that the enhancement of the catalytic activities is caused by the localized surface plasmon resonance (LSPR) effect of the Au and Au@SiO_2 NPs. With respect to their catalytic efficiency, the optimum sizes of the Au NPs are determined to be 18 nm for both the bare Au and Au@SiO_2 NPs. In addition, the Pt/TiO_2/Au@SiO_2 systems show significantly higher catalytic activities than Pt/TiO_2/Au, due to the enhanced LSPR caused by the coverage of the SiO_2 shells over the Au NPs. Particularly, Pt/TiO_2/Au18@SiO_2 exhibits the highest activity in evolving CH_4, which is estimated to be 3.1 times that of the bare Pt/TiO_2.

1. Introduction

For the last few decades, there have been increasing demands to develop new sources of clean energy on account of global warming and energy crisis resulting from the rapid increase of the atmospheric CO_2 level and depletion of fossil fuels. The conversion of CO_2 to useful organic compounds by photocatalytic treatment using inorganic catalysts is considered to be a promising strategy to solve these global issues all at once. In this respect, the design of photocatalytic systems efficiently operating under sunlight will be one of the most important subjects. However, the development of efficient catalytic systems for CO_2 conversion still remains in the embryonic stages, because CO_2 reduction reactions are thermodynamically highly endothermic and require multiple electrons and protons [1–5]. For instance, eight electrons and four protons are required to convert one molecule of CO_2 to CH_4 [6–8], while six-electrons and four protons are necessary to form a CH_3OH molecule [9,10].

In the field of semiconductor-based photocatalysts, a facile way to generate multiple electrons on the catalyst surface is the loading of noble metals on its surface. The electrons generated in the conduction band (CB) of the photocatalytic semiconductor by bandgap excitation are readily transported to the noble metals, because their Fermi levels are located relatively more positive side than the CB levels of the semiconductors. It is known that the Pt/TiO_2 system is one of the most efficient photocatalytic systems in converting CO_2 to CH_4, due to the unique catalytic role of Pt [11–18]. Under UV-light irradiation, the excited electrons in the TiO_2 CB are transported to the Pt co-catalyst, while the holes in the TiO_2 valence band (VB) can produce H^+ by water oxidation. The CO_2 adsorbed on the Pt/TiO_2 is then converted to CH_4 through the catalytic role of the Pt co-catalyst.

Noble metal nanoparticles (NPs) such as Au or Ag generate strong localized surface plasmon resonance (LSPR) when they are irradiated by a light source with a suitable wavelength. It is well-known that the strength of the LSPR in noble metal NPs is strongly dependent on their size, shape, and surface charge [19–22]. As the size of the NPs increases, the LSPR increases rapidly and the plasmon absorption band shifts toward the longer wavelength region. Moreover, plasmonic NPs with anisotropic shapes can show multiple resonant peaks, due to the multipolar resonances in different directions, depending on their aspect ratio [23,24]. Another important factor affecting the strength of the LSPR is the dielectric constant of the medium surrounding the plasmonic NPs. For instance, it is observed that the LSPR of the Au NPs increases remarkably when they are covered by a thin layer of silica or alumina [25–27].

* Corresponding author.
E-mail address: wanin@inha.ac.kr (W.I. Lee).

http://dx.doi.org/10.1016/j.apcatb.2016.06.025
0926-3373/

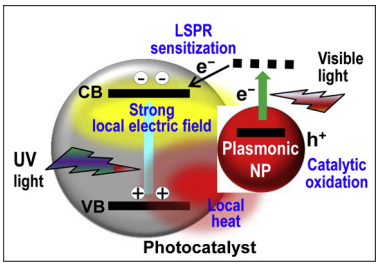

Scheme 1. Several plasmonic effects occurring in a plasmonic NP loaded photocatalyst under UV–vis light irradiation.

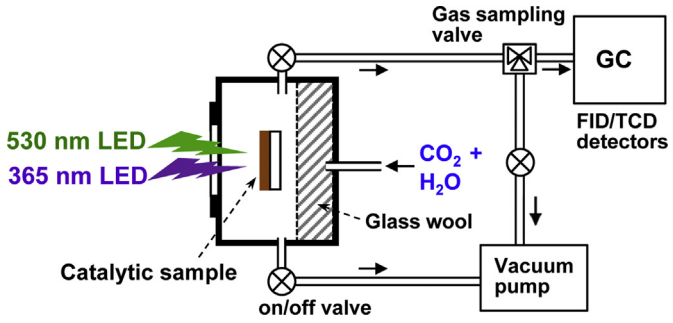

Fig. 1. Schematic diagram of the gas-tight reactor system for the photocatalytic CO_2 reduction reactions.

Thus far, there have been various reports that the photocatalytic reaction rates are enhanced by the LSPR effect of plasmonic NPs. For example, Au NPs have been applied as a catalyst or co-catalyst in several photocatalytic reactions such as the photodegradation of dyes [28–30], decomposition of organic compounds [31–35], and other photoelectrochemical reactions [21,36–38]. However, the role of the plasmonic effect in promoting photocatalytic reactions is complicated and not completely understood yet, because several specific effects are involved, as seen in Scheme 1. Upon light irradiation, a strong localized electric field is created around the plasmonic NPs, boosting the bandgap excitation for the photocatalytic semiconductors. Hence, an increased number of charge-separated electron-hole pairs will be generated on the catalyst surface, which is advantageous for photocatalytic reactions [19,39,40]. In addition, due to the electron oscillation in the plasmonic NPs upon light irradiation, local heat can be generated around the plasmonic NPs, which may contribute to boost the catalytic reactions of the main photocatalysts [19,41,42]. Another important effect is the so-called 'LSPR sensitization effect'. Plasmonic NPs can be excited by photons corresponding to the plasmonic band energy. Then the excited electrons move to the CB of the adjacent semiconductor. These electrons can be utilized for various reduction reactions [19,43–47]. In addition, the holes left in the plasmonic NPs, as a result of LSPR sensitization process, can participate in oxidation reactions. It has been reported that many organic compounds can be selectively oxidized under visible light irradiation by this strategy, because those holes have a mild oxidation power [48–51]. Contrarily, under UV–vis light irradiation, the catalytic effect of the holes from the plasmonic NPs will not be significant, because the photocatalytic oxidation reactions are dominated by the holes in the VB of photocatalytic semiconductors, revealing strong oxidation power.

Thus far, plasmonic NPs have been introduced occasionally to enhance photocatalytic CO_2 reduction reactions. Most such reports focused on plasmonic NP-loaded TiO_2 systems, which show only limited catalytic activity in CO_2 reduction reactions [45–47,52]. However, plasmonic NPs have rarely been applied to the Pt/TiO_2 system, known to be an efficient photocatalytic system in CO_2 reduction reactions [53]. Furthermore, the specific roles of individual plasmonic effects as well as the optimization strategies for the enhancement of photocatalytic CO_2 reduction reaction have not been investigated systematically. Herein, we controlled the size of the Au NPs in the range of 4–26 nm and also prepared the corresponding Au@SiO_2 coreshell NPs. They are then loaded on the surface of Pt/TiO_2, and the size-dependent LSPR effects of the Au NPs and Au@SiO_2 NPs in the photocatalytic CO_2 reduction reaction are analyzed systematically by performing the catalytic measurements under different light sources. The obtained results offer insight into the design of highly efficient plasmonic photocatalysts, as well as provide a clear understanding of the LSPR effect in the CO_2 conversion reactions.

2. Experimental

2.1. Syntheses of materials

2.1.1. Synthesis of Pt/TiO_2

Pt NPs were deposited on TiO_2 by a well-known photodeposition method. In a typical synthesis, 0.5 g of TiO_2 (Degussa P25) was suspended in a mixture of H_2O and methanol (50/50 in volume) and stoichiometric amounts of aqueous H_2PtCl_6 solution were added. Typically, to obtain the 0.3 w% Pt/TiO_2 (Pt: TiO_2 = 0.03: 0.997 in weight) sample, 1 mL of an aqueous solution containing 6.3 mg of H_2PtCl_6 was added dropwise to a suspension of 1.0 g of P25 in H_2O/MeOH (80/20 in volume). After stirring for 15 min, the suspension was irradiated with a 300 W Xe lamp (Newport, Model 66902) for 30 min while vigorous stirring. The TiO_2 suspension turned a pale gray color, suggesting the deposition of Pt on the surface of TiO_2. The prepared Pt/TiO_2 powder was collected by centrifuging the slurry, washed with a water/ethanol mixture and then dried at 80 °C for 4 h.

2.1.2. Synthesis of various Au NPs

4 nm-sized Au NP (Au4) was prepared by applying a two-phase synthesis method with minor modification [54]. In a typical experiment, 50 mL of a 10 mM $HAuCl_4$ aqueous solution was prepared and then mixed with 50 mL of toluene solution containing 25 mM tetraoctyl ammonium bromide (TOAB). After the $HAuCl_4$ was completely transferred to the toluene phase by stirring for 30 min, the toluene phase was selected. 1.65 mL of oleylamine was added to this solution and 0.283 g of $NaBH_4$ in 15 mL of H_2O was then added dropwise while vigorous stirring. The mixture turned deep red, indicating the formation of Au NPs. The prepared Au4 was precipitated by adding methanol and the collected precipitate was washed several times with methanol.

8 nm-sized Au NP (Au8) was prepared by the procedure reported by Jiménez et al. [55]. 2.2 mM sodium citrate was dissolved in 150 mL of H_2O in a round-bottomed flask and the temperature of solution was increased to 100 °C. After 1.0 mL of 25 mM $HAuCl_4$ aqueous solution was added, the reaction mixture was refluxed for 210 s. To quench the reaction, the flask was quickly dipped in an ice bath. Then, 100 mL of methanol was added to precipitate the prepared Au NPs. The collected precipitate was washed with methanol to obtain the Au8 NP.

18 and 26 nm-sized Au NPs (Au18 and Au26, respectively) were prepared by a citrate reduction method by varying the ratio of $HAuCl_4$ to sodium citrate [56]. While a 90 mL of 0.25 mM $HAuCl_4$ aqueous solution in a round-bottomed flask was refluxed at 100 °C, 45 mg of sodium citrate in 10 mL of H_2O was added to prepare Au18 (12 mg sodium citrate in 10 mL H_2O was used to obtain Au26), and the reaction mixture was refluxed for an additional 30 min. The change of the color to pink indicates the formation of the Au NPs.

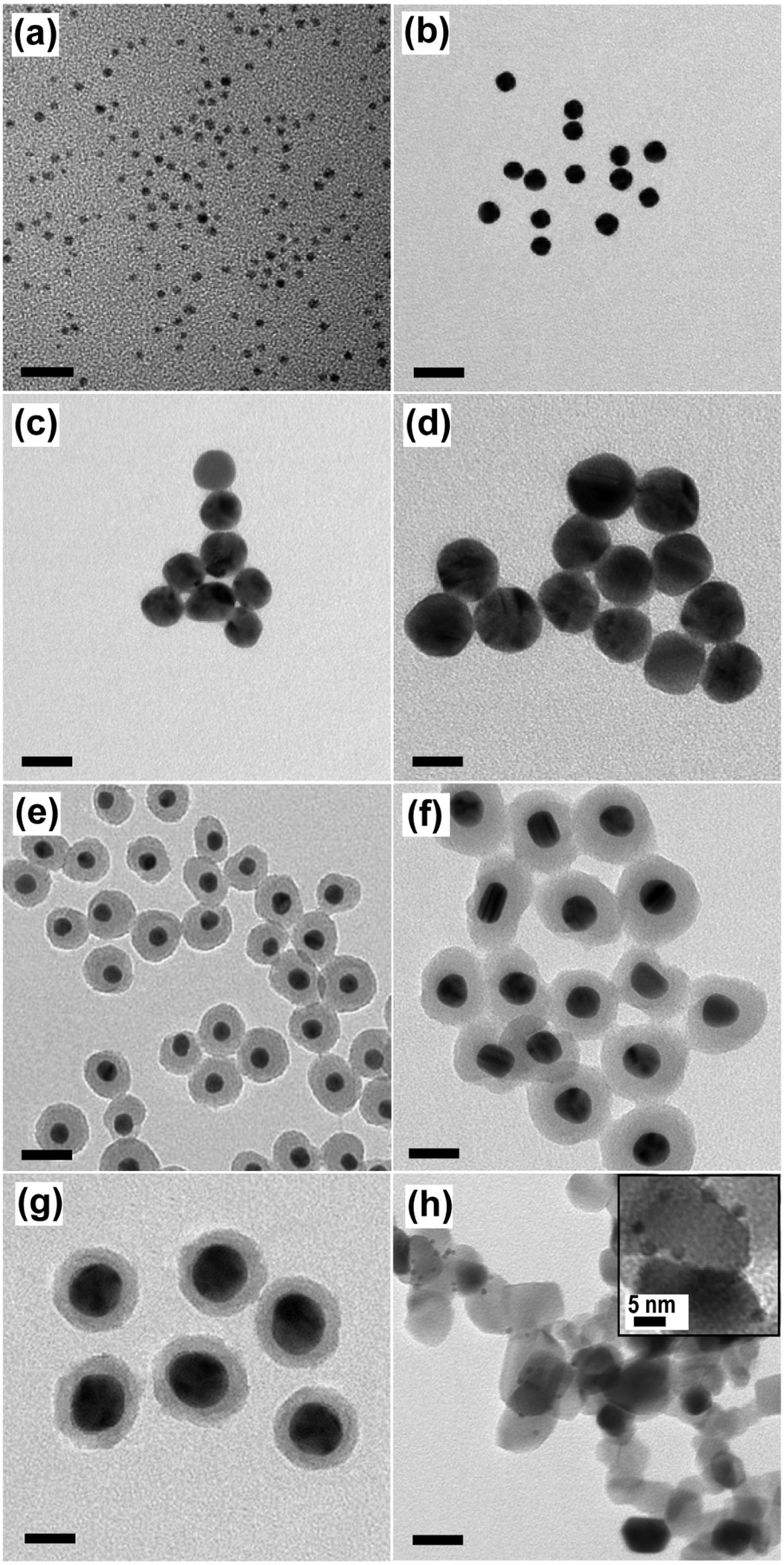

Fig. 2. TEM images of Au4 (a), Au8 (b), Au18 (c), Au26 (d) Au8@SiO_2 (e), Au18@SiO_2 (f), Au26@SiO_2 (g), and 0.3 w% Pt-loaded TiO_2 samples (h). All of the scale bars indicate 20 nm.

The prepared Au NPs were collected by centrifugation and washed with water several times.

2.1.3. Synthesis of Au@SiO_2 core-shell structures and bare SiO_2 NP

Silica was over-coated on the surfaces of Au8, Au18 and Au26 by a modified Stöber process [57]. In a typical procedure, a 300 mL stock solution of silica sol consisting of 285 mL of ethanol, 10.7 mL of H_2O, 4.27 mL of NH_4OH (28–30% in water, Aldrich), and 47.5 μL of tetraethyl orthosilicate (TEOS) (98%, Aldrich) was prepared by stirring the mixture for 30 min under ambient conditions. To obtain the Au8@SiO_2, 2 mL of the Au8 NP aqueous suspension containing 3 mg of Au was added to 75.8 mL of a silica-sol stock solution and stirred for 4 h under ambient conditions. The prepared Au8@SiO_2 NP was collected by centrifugation, washed with ethanol, and dispersed in water. To obtain Au18@SiO_2, 2 mL of an Au18 NP aqueous suspension containing 3 mg of Au was added to 56.2 mL of silica-sol stock solution, whereas 39.8 mL of silica-sol stock solution was used to prepare Au26@SiO_2.

To obtain 25 nm-sized spherical SiO_2, 100 mL of methanol, 3.5 mL of NH_4OH, and 9.0 mL of deionized water were mixed, and 6.25 mL of TEOS was subsequently added [58]. After vigorous stirring for 1 h under ambient conditions, the solution was centrifuged at 20,000 rpm to precipitate the prepared SiO_2 NP, which was washed with 2-propanol and dried at 80 °C.

2.1.4. Synthesis of Pt/TiO_2/Au, Pt/TiO_2/SiO_2@Au and Pt/TiO_2/SiO_2

0.5 g of Pt/TiO_2 powder was suspended in 20 mL of H_2O by sonication, and 50 mg of maleic acid, used as a molecular anchor between Pt/TiO_2 and the plasmonic NPs, was then added and stirred for 1 h. Stoichiometric amounts of Au, Au@SiO_2 or SiO_2 were suspended in 2 mL of water and then added dropwise to the pre-prepared Pt/TiO_2 suspension, while stirring the mixture vigorously for 2 h at 60 °C. The product was then collected by centrifugation and dried at 100 °C for 2 h. All of the as-prepared samples were irradiated by a 300 W Xe lamp (Newport, Model 66902) for 12 h to remove organic impurities present on the photocatalysts.

2.2. Characterization

Field emission transmission electron microscopy (FE-TEM) images were obtained by a JEOL JEM2100 F operated at 200 kV. One milligram of the synthesized particles was dispersed in 50 mL of ethanol, and a drop of the suspension was then spread on a holey amorphous carbon film deposited on the copper grid. UV–visible absorbance spectra was acquired using a Perkin-Elmer Lambda 40 spectrophotometer.

2.3. Evaluation of photocatalytic activity

The CO_2 reduction efficiencies of the various photocatalytic samples were evaluated by monitoring the organic compounds evolved in a home-made gas-tight reactor with an internal volume of 450 mL, as described in Fig. 1. An aqueous slurry containing 32.0 mg of the photocatalytic sample was spread uniformly on a $5 \times 5\ cm^2$ Pyrex glass and dried at 50 °C for 2 h. The prepared photocatalytic film was then placed in the center of the reactor, where its entire area is irradiated through a quartz window. Before measuring the photocatalytic activity, the film sample was irradiated by a 300 W Xe-lamp, emitting UV and visible-light, for 1 h to remove organic impurities in the catalyst. After the evacuation of the reactor, the gas-tight reactor was filled with water saturated CO_2 gas until the reactor pressure reached 780 Torr. Two LED lamps (5 W, Asahi Spectra Co., Model VCL-3Q), emitting monochromatic 365 nm and 530 nm light, respectively, were employed in designing the light sources. The gas mixtures in the reactor were magnetically convected during the irradiation. In every 30 min of irradiation, a 0.5 mL of gas sample was automatically taken from the reactor and sent to a gas chromatograph (Agilent Technologies, Model 7890N) using an auto sampling valve system. For the detection of CH_4, CH_3OH, HCHO, HCOOH, C_2H_5OH and CH_3CHO, DB-1 column (Agilent Technologies, for FID detector) was applied, whereas Supelco Carboxen-1010 column (Agilent Technologies, for TCD detector) was used for the detection of CO_2, CO and O_2.

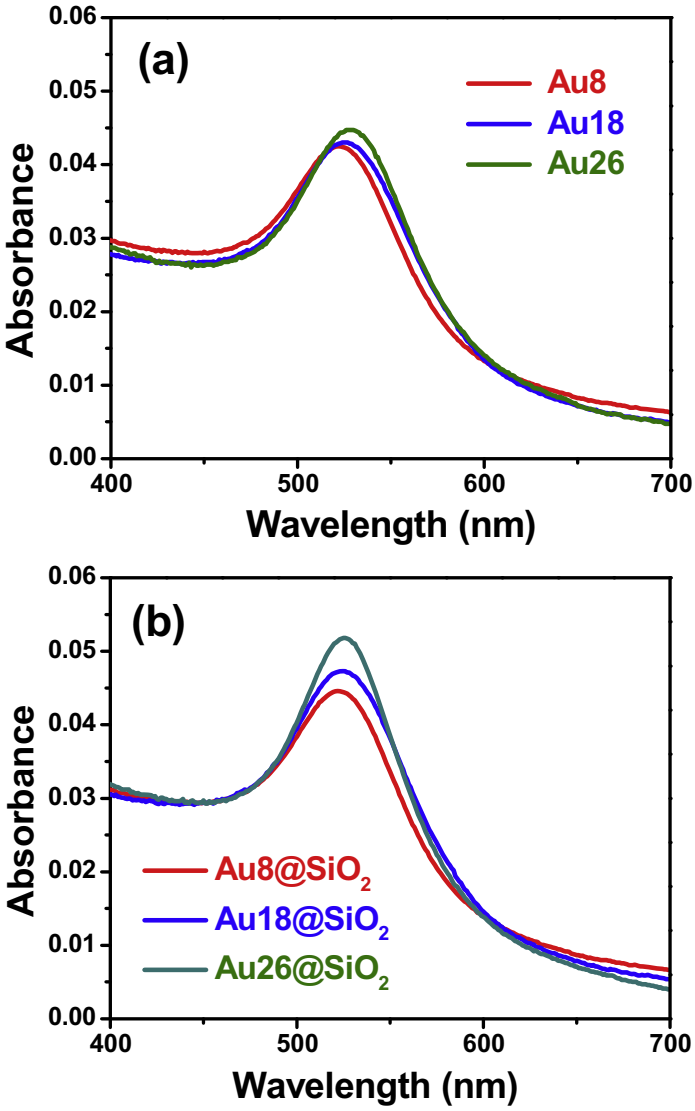

Fig. 3. UV–vis absorption spectra for the various Au NPs (a) and Au@SiO_2 NPs (b) suspended in aqueous solution. For the Au@SiO_2 NPs, the SiO_2 shell thicknesses were controlled to 8–10 nm.

3. Results and discussion

As seen in the TEM images in Fig. 2a–d, the as-prepared Au NPs show monodispersed spherical morphologies with average diameters of 4, 8, 18 and 26 nm, respectively. In order to prepare Au@SiO_2 core–shell structures, SiO_2 layer was coated on the surface of the 8, 18 and 26 nm Au NPs by a sol–gel process [57]. The TEM images of Fig. 2e–g indicate that the SiO_2 shell thicknesses of the Au@SiO_2 core–shell structures are about 8–10 nm for all of the Au NPs. The UV–visible absorption spectra of the various Au and SiO_2@Au NPs suspended in aqueous solution are shown in Fig. 3. As the size of the Au NPs increases, the plasmonic absorption peaks of the Au and

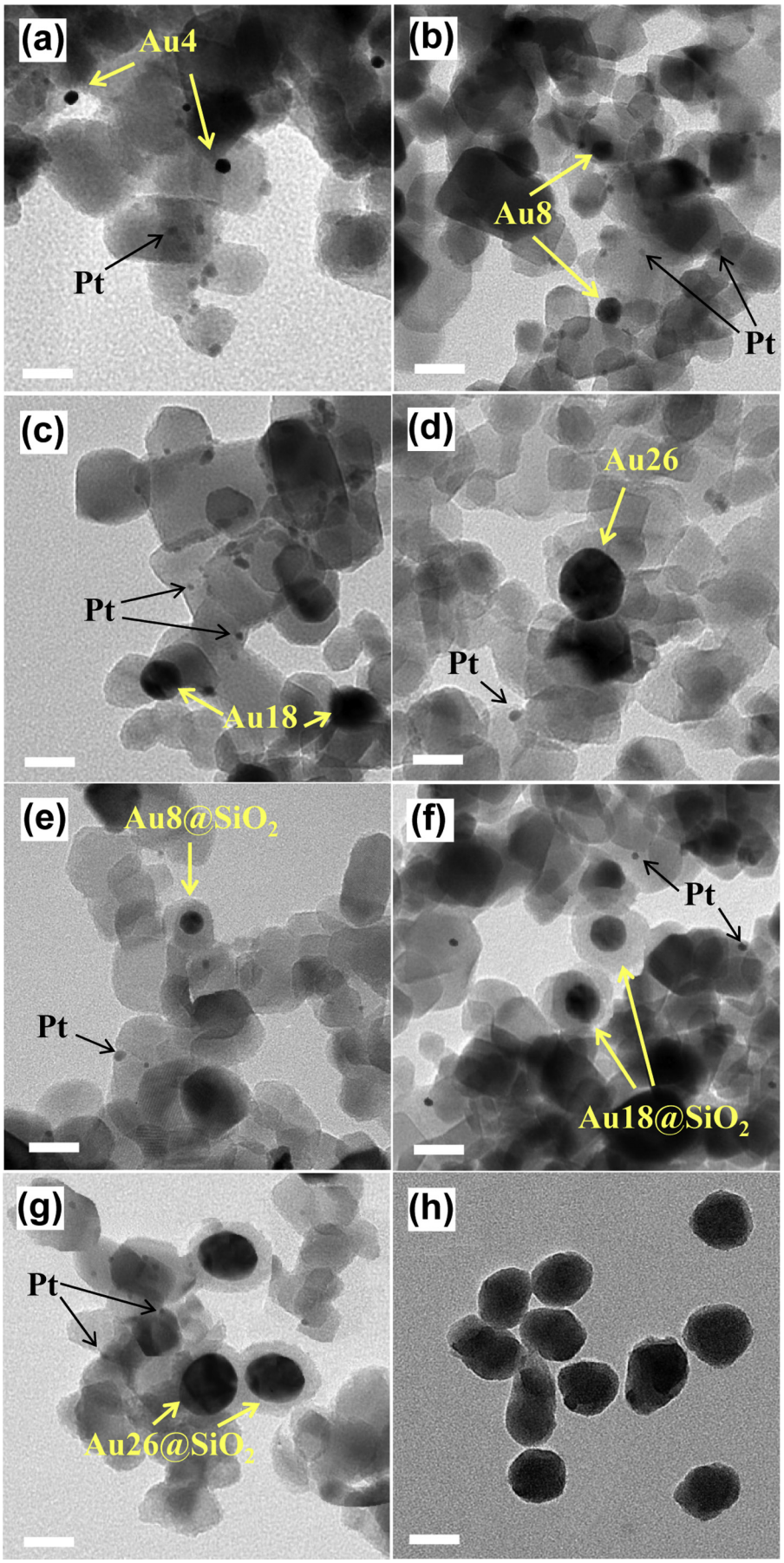

Fig. 4. TEM images of $Pt/TiO_2/Au4$ (a), $Pt/TiO_2/Au8$ (b), $Pt/TiO_2/Au18$ (c), $Pt/TiO_2/Au26$ (d), $Pt/TiO_2/Au8@SiO_2$ (e), $Pt/TiO_2/Au18@SiO_2$ (f), $Pt/TiO_2/Au26@SiO_2$ (g), and a blank SiO_2 NP(h) samples. All of the scale bars indicate 20 nm.

Au@SiO_2 NPs are slightly red-shifted, which is in good agreement with the reports in the literature [59].

The Pt/TiO_2 system is known as one of the most efficient photocatalysts for converting CO_2 to CH_4 under UV light irradiation [53]. The electrons in the CB of TiO_2 generated by bandgap excitation are transported to the Pt, and the accumulated electrons in the Pt are then utilized for the reduction reaction of CO_2, requiring eight electrons in converting a molecule of CO_2 to CH_4. In preparing Pt/TiO_2, Pt was deposited on the surface of commercial TiO_2 (Degussa P25) by a typical photodecomposition method [17]. The TEM image of the 0.3 w% Pt/TiO_2 (Pt: TiO_2 = 0.03:0.997 in weight ratio) sample, as shown in Fig. 2h and its inset, indicates that most of the deposited Pt NPs are about 3 nm in size and are uniformly spread over the TiO_2 surfaces. In order to optimize the photocatalytic activity of Pt/TiO_2, the Pt loading was varied from 0 to 0.4%. As the amount of Pt deposited on TiO_2 increases, the number of catalytic sites will increase, but excessive Pt will be detrimental to the catalytic efficiency, because the Pt NPs can act as a charge recombination center [60]. Herein, under the irradiation of a monochromatic 365 nm LED lamp, we evaluated the photocatalytic activity of the Pt/TiO_2 samples containing various Pt compositions for the conversion of CO_2 to CH_4. As shown in Fig. 1S, 0.3 w% Pt was found to provide the highest conversion rate (0.96 μmol g^{-1} h^{-1}) in evolving CH_4 from CO_2. Hence, 0.3 w% Pt/TiO_2 was chosen in preparing the various plasmonic photocatalysts in this work.

For the construction of the plasmonic photocatalysts, the prepared Au NPs or Au@SiO_2 NPs in various sizes were loaded on the Pt/TiO_2 surfaces by utilizing maleic acid as an anchoring group. Fig. 4a-d show the TEM images of Au4-deposited Pt/TiO_2 (Pt/TiO_2/Au4), Au8-deposited Pt/TiO_2 (Pt/TiO_2/Au8), Au18-deposited Pt/TiO_2 (Pt/TiO_2/Au18), and Au26-deposited Pt/TiO_2 (Pt/TiO_2/Au26), respectively, exhibiting the presence of Au NPs among the agglomerated TiO_2 NPs. Fig. 4e-g show the TEM images of the Pt/TiO_2/Au8@SiO_2, Pt/TiO_2/Au18@SiO_2, and Pt/TiO_2/Au26@SiO_2, respectively. As a control experiment, approximately 25 nm-sized spherical SiO_2 NP (see Fig. 4h) was synthesized by a sol–gel procedure without inserting the Au NPs. The prepared SiO_2 NP was then employed to fabricate the Pt/TiO_2/SiO_2 sample, which was used as a blank sample.

In order to investigate the size dependent plasmonic effect of the Au and Au@SiO_2 NPs for the photocatalytic reaction of Pt/TiO_2, two kinds of light sources were employed in this work. First, a monochromatic 365 nm LED lamp (termed as Light-I) was applied as the UV light source. Irradiation with 365 nm photons can be used for the bandgap excitation of TiO_2, but would not be suitable to activate the plasmonic Au NPs. Second, 365 nm and 530 nm LED lamps were co-irradiated (termed as Light-II) to the plasmonic photocatalysts. With the irradiation of Light-II, in addition to the bandgap excitation of TiO_2, the loaded Au NPs can be activated to generate a strong LSPR effect, because the absorption peak position of the plasmonic Au NPs is coincident with the wavelength of the photons emitted from the 530 nm LED lamp (see Fig. 3).

The influence of the plasmonic effect afforded by the Au or Au@SiO_2 NPs on the photocatalytic activity of Pt/TiO_2 will be dependent on their loading concentrations. Hence, to obtain the optimum concentration of Au NPs on the Pt/TiO_2, the evolution rate of CH_4 under Light-II was measured as a function of the amount of Au NPs loaded. As shown in Fig. S2, the optimum concentrations of Au4, Au8, Au18, and Au26 for the Pt/TiO_2/Au samples in order to maximize the evolution of CH_4 are 0.3, 0.4, 0.4, and 0.4 wt%, respectively. The optimized concentration for each type of Au NP was then employed to prepare the Pt/TiO_2/Au samples for the study of the size-dependent LSPR effects.

In addition, as a blank experiment, the reactor was filled with Ar gas and water vapor without inserting CO_2 gas. The evolved gas product by the photocatalytic reaction with Pt/TiO_2/Au18 under Light-II was then monitored. As shown in Fig. S3, no CH_4 was observed within the detection limit, confirming that the evolved CH_4 does not originate from the organic impurities that might be present in the catalytic samples.

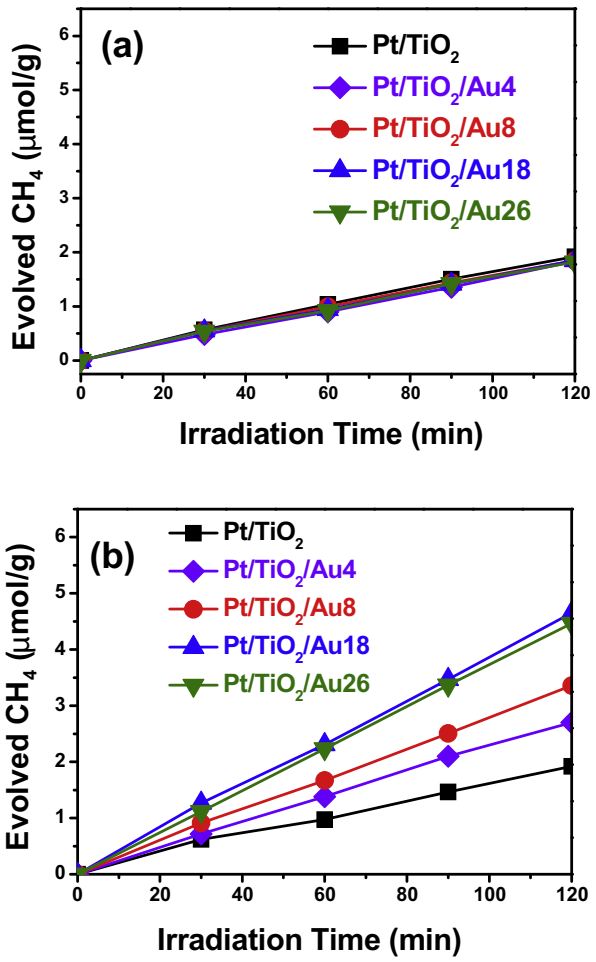

Fig. 5. CH_4 evolution as a function of irradiation time in the photocatalytic CO_2 conversion reactions with Pt/TiO_2 and various Pt/TiO_2/Au samples under 365 nm LED lamp irradiation (a) and co-irradiation of 365 nm and 530 nm LED lamps.

Fig. 5a shows the catalytic activities of the Pt/TiO_2 loaded with various Au NPs as well as that of the bare Pt/TiO_2, under the irradiation of Light-I. The loading of Au NPs, regardless of their size, did not appreciably modify the catalytic activities of Pt/TiO_2. This result indicates that the loaded Au NPs do not influence the photocatalytic reaction, because they are not activated by the 365 nm wavelength light to generate the LSPR effect. Like the Pt co-catalysts, the Au NPs loaded on TiO_2 can bring about charge separation, but it turned out that the additional charge separation caused by them does not appreciably affect the photocatalytic activity of Pt/TiO_2.

The same experiments were also performed under the irradiation of Light-II. In case of the bare Pt/TiO_2, the photocatalytic activity was not altered by changing the light source (see Fig. 5b), implying that additional visible-light does not influence the photocatalytic reaction. In contrast, however, all of the Au-loaded Pt/TiO_2 photocatalysts exhibited much higher catalytic activities than the bare Pt/TiO_2, clearly indicating that the enhancement of the photocatalytic activity is caused by the LSPR effect of the Au NPs activated by the 530 nm photons. Moreover, as the size of the Au NPs was increased from 4 nm to 18 nm, their catalytic activity for the evolution of CH_4 was gradually increased, but the additional increase of their size to 26 nm did not increase the catalytic activity any further. It is well-known that the LSPR effect increases as the size of

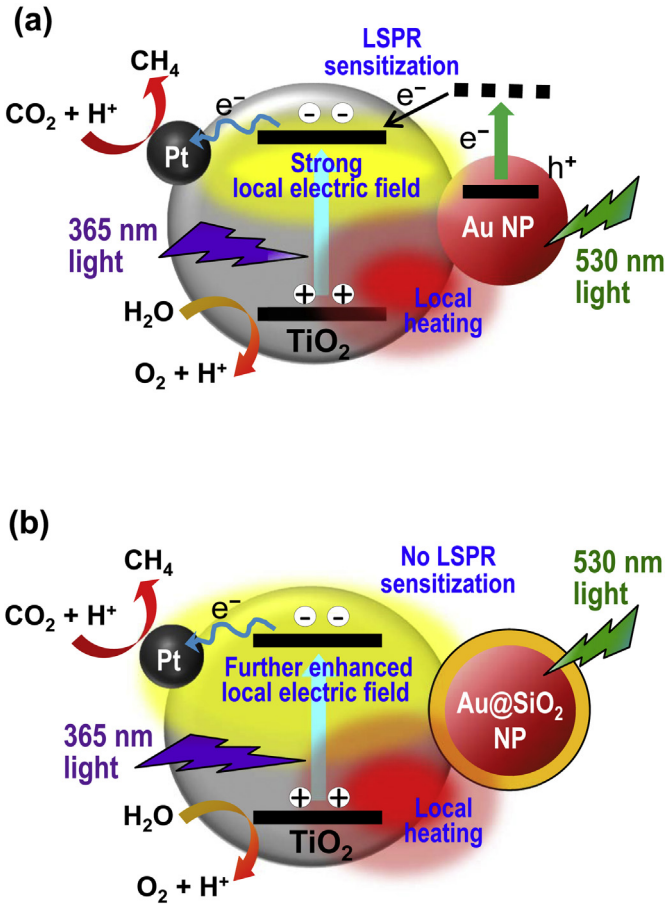

Fig. 6. Diagrams for the plasmonic effects occurring in photocatalytic $Pt/TiO_2/Au$ (a) and $Pt/TiO_2/Au@SiO_2$ (b) systems under co-irradiation of 365 nm and 530 nm LED lamps.

the Au NPs increases. In this respect, the results obtained imply that the LSPR effect of the Au NPs reaches its maximum level at a size of 18 nm.

The influence of LSPR on photocatalytic reactions is complicated, because several different effects are involved, as shown in Scheme 1 and Fig. 6a. Primarily, it promotes light absorption and produces more electron/hole pairs in TiO_2 through the enhancement of the local electric field [19,39,40]. Also, local-heat can be generated upon light irradiation, caused by the oscillation of electrons in the plasmonic NPs. Then the increased local temperature of the catalysts near the plasmonic NPs is beneficial to some catalytic reactions [19,41,42]. Moreover, the electrons in plasmonic NPs can be excited and then transported to the TiO_2 CB through the so-called LSPR sensitization effect. The transported electrons can then be utilized in several catalytic reactions [19,43–47]. Overall, the effects of LSPR would be advantageous for photocatalytic reactions, but may play different roles, depending on the specific photocatalytic reaction. For example, in the photocatalytic oxidation reactions of aqueous salicylic acid in our previous work, the Au/TiO_2 exhibited significantly higher catalytic activity than the bare TiO_2 under the irradiation of Light-II or UV–vis light [61]. In those reactions, the enhancement of the photocatalytic activity is considered to be due to the charge separation by the loaded Au NPs as well as the enhancement of the localized electric field by the LSPR effect. When the size of the Au NPs loaded on TiO_2 was increased, however, it was found that the catalytic activity was slightly decreased, although their activity values were still significantly higher than that of the bare TiO_2. The observed trend can be rationalized by the LSPR sensitization effect of Au NPs. That is, the photo-excited electrons in Au NP by visible-light can be transferred to the TiO_2 CB. These electrons would be detrimental to the oxidation reactions, because the holes in the TiO_2 VB, which are regarded to be a key component for photocatalytic oxidation reactions, can be lost by recombination with the electrons inherent in the Au NPs.

Contrarily, for reduction reactions, the LSPR sensitization effect would not be detrimental, because the electrons injected to the TiO_2 CB from the Au NPs can be utilized for the reduction reactions. Therefore, in converting CO_2 to CH_4 with $Pt/TiO_2/Au$ systems, the LSPR sensitization effect afforded by Au NPs is considered to be advantageous, because the electrons transferred from the Au NPs can be delivered to Pt, which is regarded as a catalytic site for CO_2 reduction (see Fig. 6a). Hence, we deduce that all of the individual effects caused by LSPR can promote the catalytic efficiency of CO_2 conversion, clearly explaining the observed increase of catalytic efficiency as the size of the Au NPs increased from 4 nm to 18 nm.

It has been reported that a dielectric medium surrounding the plasmonic NPs plays a significant role in enhancing the LSPR. That is, the LSPR of Au NPs can be enhanced by coating their surfaces with SiO_2 or Al_2O_3 layers [25,26]. Furthermore, by covering them with SiO_2 shell, the LSPR sensitization effect can be avoided because the dielectric SiO_2 shell blocks the charge transfer between the Au NPs and TiO_2 CB, as seen in Fig. 6b. Therefore, the effect of LSPR on the photocatalytic CO_2 reduction reaction becomes less complicated, when employing $Au@SiO_2$ NPs. Herein we tested the size-dependent LSPR effects of the $Au@SiO_2$ NPs. First of all, we determined the optimum concentration of $Au@SiO_2$ on Pt/TiO_2. As shown in Fig. S4, the photocatalytic activities of $Pt/TiO_2/Au@SiO_2$ in evolving CH_4 from CO_2 as a function of the $Au@SiO_2$ concentration was evaluated for $Au8@SiO_2$, $Au18@SiO_2$, and $Au26@SiO_2$, respectively, under an irradiation of Light-II. It was determined that the optimum amounts of $Au8@SiO_2$, $Au18@SiO_2$, and $Au26@SiO_2$ are 0.4, 0.4, and 0.5 wt%, respectively. The determined optimal concentrations were then employed to prepare $Pt/TiO_2/Au@SiO_2$ samples for the comparison of the size-dependent LSPR effects of the $Au@SiO_2$ NPs.

Fig. 7a shows the photocatalytic activities under Light-I of the various Pt/TiO_2 samples deposited with the optimum amounts of $Au8@SiO_2$, $Au18@SiO_2$ and $Au26@SiO_2$, as well as those of the bare Pt/TiO_2 and $Pt/TiO_2/SiO_2$ (0.5 wt% SiO_2). Regardless of their sizes, the loading of the $Au@SiO_2$ NPs did not change the catalytic activity of Pt/TiO_2, implying that the LSPR effect of the $Au@SiO_2$ NPs is not generated by 365 nm light irradiation. When the same experiments were performed under Light-II, as shown in Fig. 7b, all of the $Au@SiO_2$-loaded catalysts showed remarkably higher photocatalytic activity than the bare Pt/TiO_2. In particular, as the size of the Au NPs increased from 8 nm to 18 nm, the catalytic activity in evolving CH_4 was notably enhanced, but further increasing their size to 26 nm did not increase the photocatalytic activity any further. In addition, loading the bare SiO_2 NP (see Fig. 4h) did not modify the catalytic activity of Pt/TiO_2 at all, suggesting that the presence of SiO_2 on the Pt/TiO_2 surface does not affect the photocatalytic activity.

The amounts of CH_4 evolved after 2 h of catalytic reaction under Light-II employing various $Pt/TiO_2/Au$ and $Pt/TiO_2/Au@SiO_2$ samples are summarized in Fig. 8. In addition to CH_4, small amounts of CO were detected during the CO_2 conversion reactions with the plasmonic photocatalysts, but its amounts are too low to estimate the plasmonic effects in the CO evolution reaction. We also attempted to monitor other organic products such as CH_3OH, HCHO, HCOOH, C_2H_5OH and CH_3CHO, but they were not found within the detection limit of GC equipped with FID detector.

Overall, the $Pt/TiO_2/Au@SiO_2$ samples showed significantly higher efficiencies in evolving CH_4 than the $Pt/TiO_2/Au$ samples. This is definitely due to the enhanced LSPR effect afforded by the

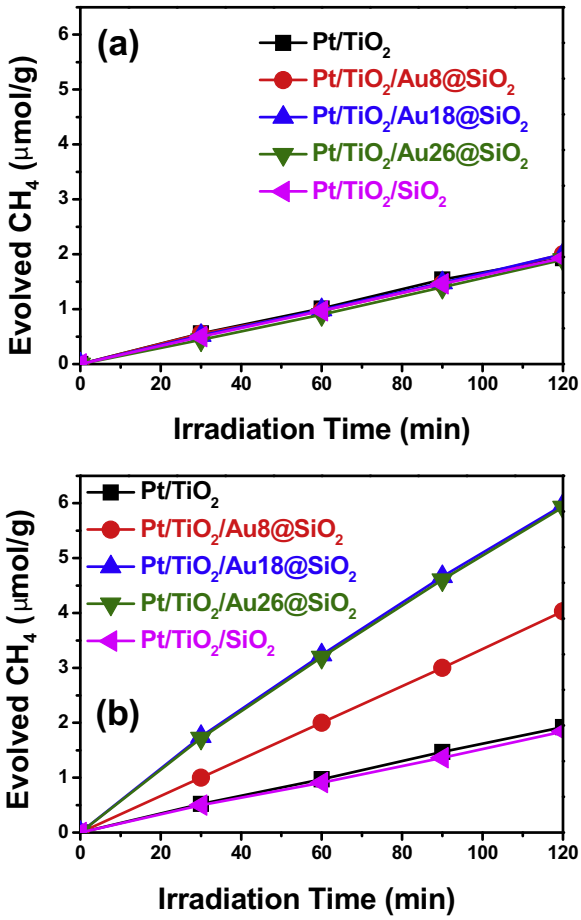

Fig. 7. CH_4 evolution as a function of irradiation time in the photocatalytic CO_2 conversion reactions with Pt/TiO_2, various $Pt/TiO_2/Au@SiO_2$ and $Pt/TiO_2/SiO_2$ samples under 365 nm LED lamp irradiation (a) and co-irradiation of 365 nm and 530 nm LED lamps (b).

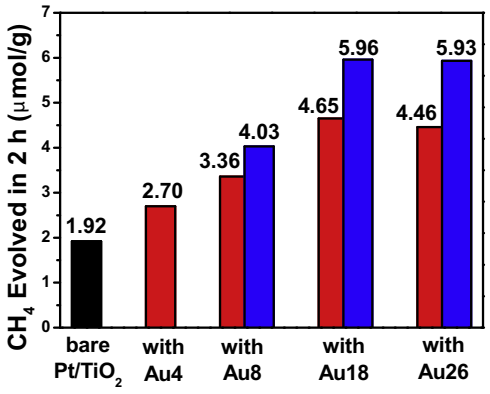

Fig. 8. Amounts of CH_4 evolved in 2 h under co-irradiation of 365 nm and 530 nm LED lamps. The red colors denote the $Pt/TiO_2/Au$ samples, and the blue colors denote the $Pt/TiO_2/Au@SiO_2$ samples. (For interpretation of the references to colour in this figure legend, the reader is referred to the web version of this article.)

coverage of the SiO_2 shells over the Au NPs. Though the LSPR sensitization effect is blocked for the $Au@SiO_2$ loaded Pt/TiO_2 system, the greatly enhanced local electric field can induce higher photocatalytic efficiencies, as illustrated in Fig. 6b. Hence, the obtained results imply that the enhancement of the local electric field is a more important factor than the LSPR sensitization in determining the CO_2 conversion reaction rate for the plasmonic photocatalysts. In addition, it was found that the catalytic activity gradually increases with increasing size of the Au NPs and reaches a maximum level at a size of 18 nm for both the $Pt/TiO_2/Au$ and $Pt/TiO_2/Au@SiO_2$ systems, suggesting that Au18 is the optimum size for their application to the plasmonic photocatalysts for converting CO_2 to CH_4. As a result, $Pt/TiO_2/Au18@SiO_2$ exhibits the highest efficiency for evolving CH_4, namely 3.1 times that of the bare Pt/TiO_2. As demonstrated in this work, the introduction of plasmonic NPs is a promising strategy for designing highly efficient CO_2 conversion photocatalysts.

4. Conclusions

Under 365 nm LED lamp irradiation, the loading of Au or $Au@SiO_2$ NPs did not appreciably change the photocatalytic activity of Pt/TiO_2 in converting CO_2 to CH_4. In contrast, under the co-irradiation of 365 and 530 nm LED lamps, their catalytic activities were remarkably enhanced, clearly indicating that this enhancement is caused by the LSPR effect of the plasmonic NPs. As the size of the Au NPs increases from 4 nm to 18 nm, the catalytic activity in evolving CH_4 gradually increased, but further increasing their size to 26 nm did not enhance the catalytic activity any further, suggesting that the LSPR effect of the Au NPs reaches its maximum level at a size of 18 nm. The same trend was observed for the $Au@SiO_2$-loaded Pt/TiO_2 catalysts, but their catalytic activities were significantly higher than those of the Au-loaded Pt/TiO_2, due to the enhanced LSPR effect by the coverage of SiO_2 shells over Au NPs. It was also found that the LSPR sensitization effect is advantageous for the photocatalytic CO_2 reduction reaction, in contrast to the photocatalytic oxidation reaction.

Acknowledgments

This work was supported by the National Research Foundation of Korea (NRF) (NRF-2015R1D1A1A01057390) and the Korea Center for Artificial Photosynthesis (KCAP) funded by the Ministry of Science, ICT and Future Planning through the NRF (No. 20090093883).

Appendix A. Supplementary data

Supplementary data associated with this article can be found, in the online version, at http://dx.doi.org/10.1016/j.apcatb.2016.06.025.

References

[1] Y. Kohno, H. Hayashi, S. Takenaka, J. Photochem. Photobiol. A 126 (1999) 117–123.
[2] J. Mao, K. Li, T. Peng, Catal. Sci. Technol. 3 (2013) 2481–2498.
[3] O. Ola, M.M. Maroto-Valer, J. Photochem. Photobiol. C 24 (2015) 16–42.
[4] V.P. Indrakanti, J.D. Kubicki, H.H. Schobert, Energy Environ. Sci. 2 (2009) 745–758.
[5] S.C. Roy, O.K. Varghese, M. Paulose, C.A. Grimes, ACS Nano 4 (2010) 1259–1278.
[6] N.M. Dimitrijevic, B.K. Vijayan, O.G. Poluektov, T. Rajh, K.A. Gray, H. He, P. Zapol, J. Am. Chem. Soc. 133 (2011) 3964–3971.
[7] A. Dhakshinamoorthy, S. Navalon, A. Corma, H. Garcia, Energy Environ. Sci. 5 (2012) 9217–9233.
[8] K. Mori, H. Yamashita, M. Anpo, RSC Adv. 2 (2012) 3165–3172.
[9] S.N. Habisreutinger, L. Schmidt-Mende, J.K. Stolarczyk, Angew. Chem. Int. Ed. 52 (2013) 7372–7408.
[10] W. Fan, Q. Zhang, Y. Wang, Phys. Chem. Chem. Phys. 15 (2013) 2632–2649.
[11] W.-N. Wang, W.-J. An, B. Ramalingam, S. Mukherjee, D.M. Niedzwiedzki, S. Gangopadhyay, P. Biswas, J. Am. Chem. Soc. 135 (2012) 11276–11281.
[12] K. Maeda, K. Domen, J. Phys. Chem. Lett. 1 (2010) 2655–2661.
[13] X. Zhang, F. Han, B. Shi, S. Farsinezhad, G.P. Dechaine, K. Shankar, Angew. Chem. Int. Ed. 51 (2012) 12732–12735.
[14] K. Tennakone, Sol. Energy Mater. Sol. Cells 10 (1984) 235–238.
[15] O. Ishitani, C. Inoue, Y. Suzuki, T. Ibusuki, J. Photochem. Photobiol. A 72 (1993) 269–271.

[16] J. Mao, L. Ye, K. Li, X. Zhang, J. Liu, T. Peng, L. Zan, Appl. Catal. B 144 (2014) 855–862.
[17] S. Xie, Y. Wang, Q. Zhang, W. Deng, Y. Wang, ACS Catal. 4 (2014) 3644–3653.
[18] S. Xie, Y. Wang, Q. Zhang, W. Fan, W. Deng, Y. Wang, Chem. Commun. 49 (2013) 2451–2453.
[19] X. Zhang, Y.L. Chen, R.S. Liu, D.P. Tsai, Rep. Prog. Phys. 76 (2013) 046401–046442.
[20] M.K. Kumar, S. Krishnamoorthy, L.K. Tan, S.Y. Chiam, S. Tripathy, H. Gao, ACS Catal. 1 (2011) 300–308.
[21] D.B. Ingram, S. Linic, J. Am. Chem. Soc. 133 (2011) 5202–5205.
[22] P. Christopher, D.B. Ingram, S. Linic, J. Phys. Chem. C 114 (2010) 9173–9177.
[23] X. Huang, I.H. El-Sayed, W. Qian, M.A. El-Sayed, J. Am. Chem. Soc. 128 (2006) 2115–2120.
[24] J.J. Mock, M. Barbic, D.R. Smith, D.A. Schultz, S. Schultz, J. Chem. Phys. 116 (2002) 6755–6759.
[25] K. Awazu, M. Fujimaki, C. Rockstuhl, J. Tominaga, H. Murakami, Y. Ohki, N. Yoshida, T. Watanabe, J. Am. Chem. Soc. 130 (2008) 1676–1680.
[26] K.L. Kelly, E. Coronado, L.L. Zhao, G.C. Schatz, J. Phys. Chem. B 107 (2003) 668–677.
[27] S. Sun, W. Wang, L. Zhang, M. Shang, L. Wang, Catal. Commun. 11 (2009) 290–293.
[28] S. Kamimura, T. Miyazaki, M. Zhang, Y. Li, T. Tsubota, T. Ohno, Appl. Catal. B 180 (2016) 255–262.
[29] P. Wang, B. Huang, Y. Daia, M.H. Whangbo, Phys. Chem. Chem. Phys. 14 (2012) 9813–9825.
[30] J. Jiang, H. Li, L. Zhang, Chem. Eur. J. 18 (2012) 6360–6369.
[31] P. Christopher, H. Xin, S. Linic, Nat. Chem. 3 (2011) 467–472.
[32] M.V. Dozzi, L. Prati, P. Canton, E. Selli, Phys. Chem. Chem. Phys. 11 (2009) 7171–7180.
[33] M. Alvaro, B. Cojocaru, A.A. Ismail, N. Petrea, B. Ferrer, F.A. Harraz, V.I. Parvulescu, H. Garcia, Appl. Catal. B 99 (2010) 191–197.
[34] E. Kowalska, O.O.P. Mahaney, R. Abe, B. Ohtani, Phys. Chem. Chem. Phys. 12 (2010) 2344–2355.
[35] G. Schubert, A. Gazsi, F. Solymosi, J. Catal. 313 (2014) 127–134.
[36] Z. Liu, W. Hou, P. Pavaskar, M. Aykol, S.B. Cronin, Nano Lett. 11 (2011) 1111–1116.
[37] J.J. Chen, C.S. Jeffrey, P.C. Wu, D.P. Wu, Tsai, J. Phys. Chem. C 115 (2011) 210–216.
[38] S.S. Rayalu, D. Jose, M.V. Joshi, P.A. Mangrulkar, K. Shrestha, K. Klabunde, Appl. Catal. B 142–143 (2013) 684–693.
[39] V.P. Zhdanov, C. Hagglund, B. Kasemo, Surf. Sci. 599 (2005) L372–L375.
[40] T. Torimoto, H. Horibe, T. Kameyama, K. Okazaki, S. Ikeda, M. Matsumura, A. Ishikawa, H. Ishihara, J. Phys. Chem. Lett. 2 (2011) 2057–2062.
[41] C. Wang, O. Ranasingha, S. Natesakhawat, P.R. Ohodnicki Jr., M. Andio, J.P. Lewis, C. Matranga, Nanoscale 5 (2013) 6968–6974.
[42] L. Huimin, M. Xianguang, D.T. Duy, Z. Huabin, L. Peng, C. Kun, W. Tao, L. Mu, N. Tadaaki, Y. Jinhua, Angew. Chem. Int. Ed. 54 (2015) 11545–11549.
[43] S.T. Kochuveedu, D.P. Kim, D.H. Kim, J. Phys. Chem. C 116 (2012) 2500–2506.
[44] D. Chen, X. Zhang, A.F. Lee, J. Mater. Chem. A 3 (2015) 14487–14516.
[45] W. Hou, W.H. Hung, P. Pavaskar, A. Goeppert, M. Aykol, S.B. Cronin, ACS Catal. 1 (2011) 929–936.
[46] B. Tahir, N.A.S. Amin Tahir, Appl. Surf. Sci. 356 (2015) 1289–1299.
[47] B.D. Mankidy, B. Joseph, V.K. Gupta, Nanotechnology 24 (2013) 405402–405410.
[48] X. Chen, H.Y. Zhu, J.C. Zhao, Z.F. Zheng, X.P. Gao, Angew. Chem. Int. Ed. 47 (2008) 5353–5356.
[49] A. Furube, L. Du, K. Hara, R. Katoh, M. Tachiya, J. Am. Chem. Soc. 129 (2007) 14852–14853.
[50] M. Xiao, R. Jiang, F. Wang, C. Fang, J. Wang, J.C. Yu, J. Mater. Chem. A 1 (2013) 5790–5805.
[51] H. Cheng, K. Fuku, Y. Kuwahara, K. Mori, H. Yamashita, J. Mater. Chem. A 3 (2015) 5244–5258.
[52] W. Tu, Y. Zhou, H. Li, P. Li, Z. Zou, Nanoscale 7 (2015) 14232–14236.
[53] Z. Zhang, Z. Wang, S.W. Cao, C. Xue, J. Phys. Chem. C 117 (2013) 25939–25947.
[54] M. Brust, M. Walker, D. Bethell, D.J. Schiffrin, R. Whyman, J. Chem. Soc. Chem. Commun. (1994) 801–802.
[55] I.O. Jiménez, F.M. Romero, N.G. Bastús, V. Puntes, J. Phys. Chem. C 114 (2010) 1800–1804.
[56] P. Zhao, N. Li, D. Astruc, Coord. Chem. Rev. 257 (2013) 638–665.
[57] Z. Wu, J. Liang, X. Ji, W. Yang, Colloids Surf. A 392 (2011) 220–224.
[58] T. Chung, S.-Y. Lee, E.Y. Song, H. Chun, B. Lee, Sensors 11 (2011) 10907–10929.
[59] S. Link, M.A. El-Sayed, J. Phys. Chem. B 103 (1999) 8410–8426.
[60] T. Sreethawong, S. Yoshikawa, Catal. Commun. 6 (2005) 661–668.
[61] S.M. Yoo, S.B. Rawal, J.E. Lee, J. Kim, H.-Y. Ryu, D.-W. Park, W.I. Lee, Appl. Catal. A 499 (2015) 47–54.